Self-consistent band structures, charge distributions, and optical-absorption spectra in MgO, α-Al_2O_3, and $MgAl_2O_4$

Yong-Nian Xu and W. Y. Ching
Department of Physics, University of Missouri–Kansas City, Kansas City, Missouri 64110
(Received 13 September 1990)

The electronic structures, the charge-density distributions, and the optical-absorption spectra in MgO, α-Al_2O_3, and $MgAl_2O_4$ crystals are studied by means of the first-principles self-consistent orthogonalized linear combination of atomic orbitals method. The calculated band structures of MgO and α-Al_2O_3 are compared with experimental data and previous calculations. It is concluded that the electronic structure and optical properties of the spinel $MgAl_2O_4$ cannot be taken as a simple average of that of MgO and α-Al_2O_3. By direct space integration of the calculated charge, it is shown that the ionic nature of these crystals should be best described by the formulas $Mg^{1.83+}O^{1.83-}$, $Al_2^{2.63+}O_3^{1.75-}$, and $Mg^{1.79+}Al_2^{2.63+}O_4^{1.76-}$. The charge-density maps also reveal that there are open channels of very low electron density in $MgAl_2O_4$, which may be important in ionic conductivity. The calculated optical dielectric functions for the three crystals are compared with recent vacuum ultraviolet data for an energy range up to 40 eV and show good overall agreement. The existence of an excitonic peak near the absorption edge tends to sharpen the edge, thereby increasing the gap as compared with the one-electron local-density calculations. For absorption spectra beyond the excitonic peak, most of the experimentally resolved structures are reproduced by the calculations without the need of an adjustment to widen the gap. It appears that the high conduction-band states in these three crystals, calculated by using the local-density approximation, are reasonably accurate.

I. INTRODUCTION

MgO and α-Al_2O_3 are important ceramic oxides that have been subjected to numerous experimental and theoretical studies.[1,2] They have high melting points, low coefficients of expansion, and small thermal conductivities. There is also an increasing trend in using MgO and α-Al_2O_3 as substrate materials for thin-film growth and as optical materials. MgO is highly ionic and has a simple NaCl-type structure. Its band structure has been studied by various methods[3–13] and is reasonably well established. Still, there are differences with regards to the size of the band gap, valence-band (VB) width, and values of effective charges on each ion.[13] α-Al_2O_3, on the other hand, has a much more complicated corundum structure. Several calculations were performed in the past on its band structure.[14–18] Most of these calculations were non-self-consistent or semiempirical in nature. α-Al_2O_3 has also been studied in the form of small clusters.[19–21] A recent study on the band structure of α-Al_2O_3 used a self-consistent pseudofunction method.[1] That study concentrated on the interpretation of experimental reflectivity data in terms of critical point analysis and does not provide detailed analysis of the electronic-structure and charge-density distribution. A closely related crystal to MgO and Al_2O_3 is the spinel $MgAl_2O_4$ with a complex cubic structure. Spinel oxides form a large class of inorganic solids with similar structures.[22] We are not aware of any electronic-structure study on the spinel phase.

In this paper we present the results of calculations on the electronic structures of MgO, α-Al_2O_3, and $MgAl_2O_4$ using the first-principles orthogonalized linear combination of atomic orbitals method (OLCAO) in the local-density approximation (LDA) within the density-functional formalism. The band structures, total and partial density of states (DOS), charge-density distributions, and effective charges on each ion are studied in detail. We have calculated the interband optical conductivities, or equivalently the linear dielectric functions of the three crystals up to a high photon energy of 40 eV. The results are compared with recent experimental data from vacuum ultraviolet (VUV) measurements,[1,2] using a laser plasma light source. Such comparisons provide a direct assessment on the accuracy of the band structures especially for the higher conduction bands (CB). We also show that the electronic and the optical properties of the spinel phase $MgAl_2O_4$ cannot be taken as a simple weighted superposition of that of the MgO and α-Al_2O_3 crystals.

This paper is organized as follows: In Sec. II, the structures of the three crystals are briefly discussed focusing on the relative short-range orders and interatomic distances. This is followed by a brief outline of the method of calculation in Sec. III. Results on band structures and DOS are presented in Sec. IV. Detailed analysis on the charge-density distributions and optical absorptions are presented and discussed in Secs. V and VI, respectively. Some discussion and concluding remarks are given in Sec. VII.

II. CRYSTAL STRUCTURES

The structures of the three crystals used in the present calculation and their interionic distances are summarized

in Table I. Since MgO has a very simple rocksalt structure which consists of an interpenetrating fcc lattices of Mg and O ions, there is no need for any discussion. For α-Al_2O_3, a detailed description of the crystal structure has been given by Batra.[16] α-Al_2O_3 has a corundum structure with a trigonal (or rhombohedral) unit cell containing two Al_2O_3 molecules. The coordinates of the atoms are such that an Al atoms is surrounded by six O atoms of two different nearest-neighbor (NN) distances and each O atom has four NN Al atoms. The corundum structure can also be visualized as a hexagonal cell having six layers of close-packed O atoms with the smaller Al atom located inside the octahedrally coordinated holes.[22] In this picture, the unit cell for the hexagonal lattice will be three times as large as the rhombohedral cell.

The spinel phase represents the structure of a large number of ceramic oxides.[22] It has a face-centered-cubic lattice (space group O_h^7) with eight formula units per cubic cell. Inside the cell, each Mg ion is tetrahedrally coordinated to four O atoms while each Al atom is surrounded by six octahedrally distributed O atoms. The structure is best described as a cube consisting of eight constants of type I and type II as shown in Fig. 1(a). The type-I octants contain Mg ions in tetrahedral coordination as shown in Fig. 1(b); and the type-II octants contain Al ions in octahedral coordination as shown in Fig. 1(c). In a normal spinel such as $MgAl_2O_4$, the divalent ion (Mg^{2+}) is in the type-I octant and the trivalent ion (Al^{3+}) is in the type-II octant. In an inverse spinel such as $NiFe_2O_4$, the type-I octants contain half of the trivalent ions while the type-II octants contain all the divalent ions and the other half of the trivalent ions. The distribution of cations can actually be intermediate between the normal and the inverse spinels to give a random spinel characterized by a parameter λ. λ represents the fraction of the 16 available trivalent-ion sites in type-II octants occupied by divalent ions. λ ranges from 0 for the normal spinel to 0.5 for the inverse spinel. In many systems, voids can be treated as a trivalent ion to form what is called a defect inverse spinel such as in γ-Fe_2O_3 (maghemite) or γ-Al_2O_3. The rich variety of structural configurations in spinels gives rise to very different electronic and magnetic properties among different spinel compounds.[22]

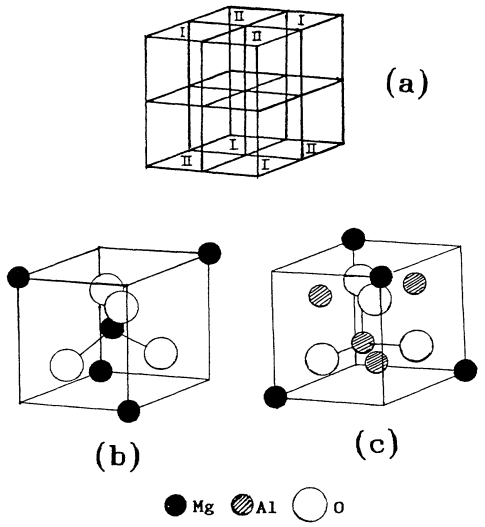

FIG. 1. Crystal structure of $MgAl_2O_4$. (a) Cubic cell showing eight constants of type I and II. (b) Type-I octant with a Mg ion in tetrahedral coordination with O; (c) type-II octant with Al ions in octahedral coordination with O.

III. METHOD OF CALCULATION

The self-consistent OLCAO method for the electronic-structure calculation of solids has been described in several recent publications.[23–29] We will only outline the major steps in the present calculation. The basis functions for the expansion of the crystal Bloch functions are linear combinations of atomic orbitals of O ($1s, 2s, 2p_x, 2p_y, 2p_z, 3s, 3p_x, 3p_y, 3p_z$), Mg, and Al ($1s, 2s, 2p_x$, $2p_y, 2p_z, 3s, 3p_x, 3p_y, 3p_z$, $4s, 4p_x, 4p_y, 4p_z, 3d_{xy}$, $3d_{yz}, 3d_{zx}, 3d_{x^2-y^2}, 3d_{3z^2-r^2}$) as appropriate for each crystal. The atomic orbitals are expressed as the linear combinations of Gaussian-type orbitals (GTO). This basis set is generally referred to as a full basis because it consists of all the valence-shell orbitals of the atoms in the crystal plus another shell of empty orbitals. The crystal potentials are constructed according to the usual local-density-functional formalism[30] with the Wigner interpolation formula for correlation correction. The potential and charge densities are each expressed as a sum of atom-centered Gaussian functions with the coefficients of the expansion determined by linearly fitting to the numerically evaluated data. The quality of the fitting is closely monitored to ensure an accurate representation of the charge density and the potential by the fitting functions. To reduce the size of the secular equation, the matrix ele-

TABLE I. Crystal-structure information of MgO, α-Al_2O_3, and $MgAl_2O_4$.

	MgO	α-Al_2O_3	$MgAl_2O_4$
Crystal structure	NaCl	Corundum	Spinel
Lattice constant	$a=4.213$ Å	$a=5.128$ Å $\beta=55.333°$	$a=8.063$ Å
Space group	$B1$	D_{3d}^6	O_h^7
Nearest-neighbor distance (Å)			
Mg-O	2.1015 (6)		1.9187 (4)
Al-O		1.9692 (3) 1.8570 (3)	1.9293 (6)

ments of the Hamiltonian and the overlap involving core orbitals are eliminated by the orthogonalization procedure. Self-consistency is generally achieved in less than 20 iterations with the eigenvalues stabilized to less than 0.0001 eV. After the self-consistency in the potential has been obtained, the eigenvalues and the eigenvectors of the band secular equations are solved at 89, 308, and 89 **k** points in the irreducible portion of the Brillouin zone (BZ) for MgO, α-Al_2O_3, and $MgAl_2O_4$, respectively. The energies and wave functions at these **k** points are used to evaluate the DOS and the optical conductivities using the linear analytic tetrahedron method.[31] The calculation of optical conductivity includes the effects of the **k**-dependent moment matrix elements. The method for the optical conductivity calculation in oxides has been described before.[27,28,32]

IV. BAND STRUCTURE AND DENSITY OF STATES

A. MgO

The calculated band structure and the DOS for MgO are shown in Figs. 2 and 3, respectively. Also shown are the projected partial DOS (PDOS) for the O and Mg atoms. The calculated band gap of 4.19 eV is direct at Γ, smaller than the reported experimental gap of 7.5 eV, and close to the other recent calculations (see Table II). The upper VB has a two-peak structure, a sharp one at -4.5 eV and a broader one centered at -1.2 eV. The total width of the upper VB is about 5.4 eV. This is in good agreement with experiment.[33,34] Other recent calculations gave a narrower bandwidth than our result. The lower O 2*s* band is 1.9 eV wide and peaks at -15.4 eV at the leading edge of the band. The CB also has a two-peak structure, one at 8.9 eV and a sharper one at 12.3 eV. There is a substantial degree of hybridization between Mg and O states. The two CB structures are the antibonding counterparts of the two bonding structures in the VB. The effective masses of the CB and the VB are also estimated from the band curvatures. The isotropic electron effective mass m^* at Γ is $0.35m_e$. The top of the VB is triply degenerate, so the hole effective masses are not isotropic. Their components are listed in Table II with an average value of $-2.60m_e$ for the heavy hole and $-0.33m_e$ for the light hole.

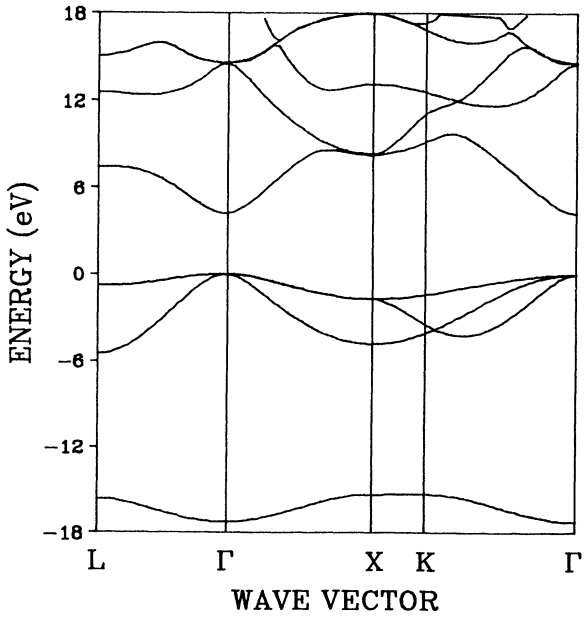

FIG. 2. Band structures of MgO.

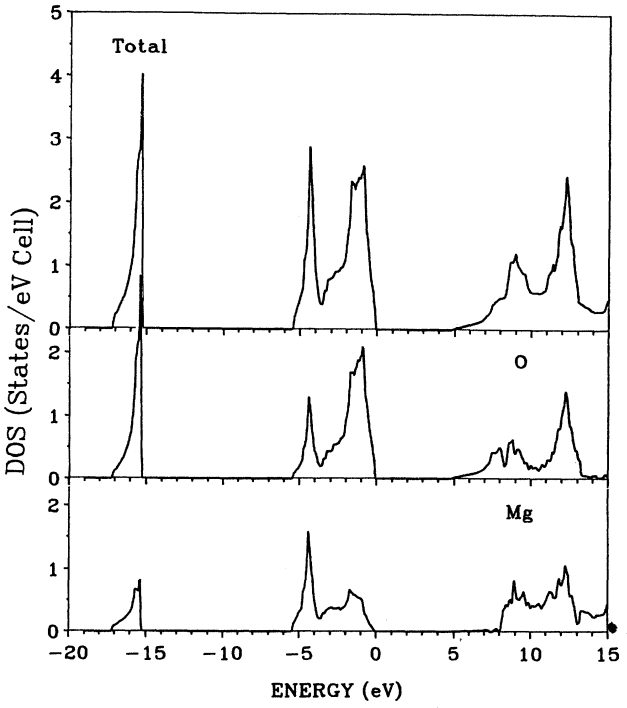

FIG. 3. DOS and PDOS of MgO.

B. α-Al_2O_3

The calculated band structure for α-Al_2O_3 in the trigonal lattice is shown in Fig. 4. The corresponding DOS

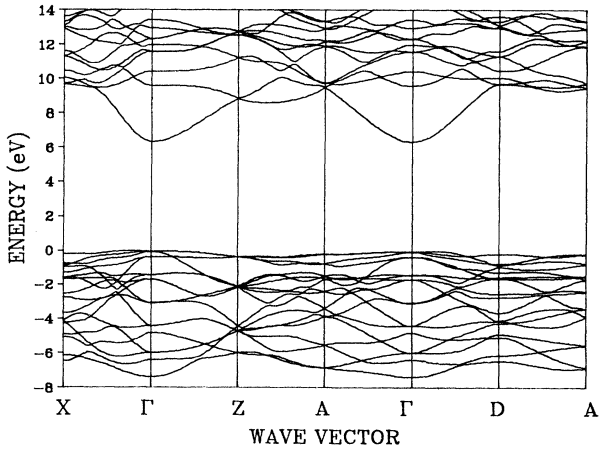

FIG. 4. Band structure of α-Al_2O_3.

and PDOS are shown in Fig. 5. Unlike MgO, the calculated band gap for α-Al_2O_3 is indirect and equal to 6.29 eV. This value is almost identical to the 6.3 eV obtained by the pseudofunction calculation.[1] The bottom of the CB is at Γ and the top of the VB is at a point of 0.20 of ΓX from Γ. However, the energy at Γ is only 0.06 eV lower than the top of the VB. So for any practical purposes, we may regard α-Al_2O_3 as a direct gap insulator. The reported experimental gap value for α-Al_2O_3 is 8.7 eV.[1,2] There are many more structures in the DOS curve reflecting an increased complexity of the crystal structure. The width of the upper VB is 7.3 eV which is significantly wider than that of MgO. The lower O 2*s* bandwidth is as wide as 3.3 eV which peaks at the leading edge of the band at -16 eV. Also, shown in Fig. 4 as dotted lines, is the VB x-ray photoemission spectroscopy (XPS) data of Ref. 35. The agreement is quite good except that there was a shoulderlike structure at about -10 eV in the data that is not present in the calculated DOS. This structure is likely to be due to surface contamination in the sample. More recent data by polarized x-ray-emission spectroscopy shows no such structure.[36]

The effective-mass components of the CB along different directions of BZ edges are listed in Table II with an average value of about $0.35m_e$. The hole effective masses are huge because of the very flat top of the VB. At the Γ point, the top of the VB consists of hybridized orbitals of O 2*p* and Al 3*p*. The lowest CB is nondegenerate with mixed Al 3*s*, O 2*s*, and O 3*s* characters. We do not find any significant participation of the Al 3*d* orbitals for the CB states with energy less than 11 eV, i.e., about 5 eV from the CB minimum.

C. $MgAl_2O_4$

The band structure and the DOS for the spinel $MgAl_2O_4$ are displayed in Figs. 6 and 7, respectively. Like α-Al_2O_3, the calculated band gap is indirect and equal to 6.51 eV. The quoted experimental gap is 7.8 eV.[2] The bottom of the CB is at Γ but the top of the VB is at a point 0.20 along Γ-*K*. The energy difference between this point and Γ is even smaller, less than 0.004 eV. So the top of the VB is again very flat. The CB minimum at Γ is nondegenerate and composed of the *s* orbitals of

TABLE II. Calculated band-structure information on MgO, α-Al_2O_3, and $MgAl_2O_4$.

	MgO	α-Al_2O_3	$MgAl_2O_4$
Band gap (eV)	direct (Γ)	indirect	indirect
Calc. (present)	4.19	6.29	6.51
(others)	4.65,[a] 4.50,[b] 4.87[c]	6.3,[d] 8.0[e]	
Experiment	7.58,[d] 7.8[f]	8.7[g], 9.4[h]	7.8[g]
Upper VB width (eV)			
Calc. (present)	5.50	7.39	5.32
(others)	5.1,[i] 4.48[a], 4.80[b], 4.75[c]	8.1,[d] 6.0[e]	
Experiment	6.5[j], 5–6[k]		
O 2*s* bandwidth (eV)	1.96	3.26	2.55
Calc. (present)	1.96	3.26	2.55
Gap between upper VB and O 2*s* bands (eV)	9.81	8.53	9.52
Effective mass (m_e)			
Electron	0.35 ($\Gamma\rightarrow L$)	0.16 ($\Gamma\rightarrow X$)	0.44 ($\Gamma\rightarrow L$)
	0.35 ($\Gamma\rightarrow X$)	0.45 ($\Gamma\rightarrow Z$)	0.44 ($\Gamma\rightarrow X$)
	0.35 ($\Gamma\rightarrow K$)	0.40 ($\Gamma\rightarrow A$)	0.44 ($\Gamma\rightarrow K$)
		0.38 ($\Gamma\rightarrow D$)	
Heavy hole	-2.77 ($\Gamma\rightarrow L$)	large	large
	-1.60 ($\Gamma\rightarrow X$)		
	$-4.10, -1.80$ ($\Gamma\rightarrow K$)		
Light hole	-0.31 ($\Gamma\rightarrow L$)		
	-0.35 ($\Gamma\rightarrow X$)		
	-0.32 ($\Gamma\rightarrow K$)		
$\epsilon(0)$	4.28	3.86	6.07

[a]Reference 11.
[b]Reference 9.
[c]Reference 8.
[d]Reference 1.
[e]Reference 16.
[f]Reference 40.
[g]Reference 2.
[h]Reference 43.
[i]Reference 13.
[j]Reference 34.
[k]Reference 33.

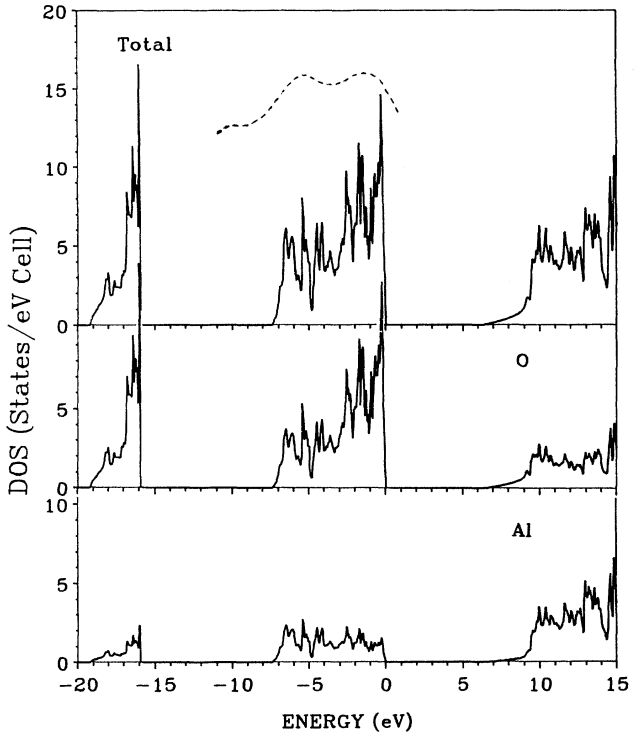

FIG. 5. DOS and PDOS of α-Al_2O_3.

all the atoms in the cell. The electron effective mass is $0.44m_e$, slightly larger than that in MgO and the hole effective mass is large similar to α-Al_2O_3. The upper VB has a total width of about 5.3 eV which is smaller than that of MgO and much smaller than α-Al_2O_3. The DOS for this band has many structures due to the complexity of the crystal with major peaks at -0.5, -1.2, -2.4, -3.7 and -4.5 eV. The major feature of the CB DOS is a peak at 13.5 eV and a very deep minimum at 12.3 eV. The general shape of the DOS appears to be intermediate between MgO and α-Al_2O_3. The lower O $2s$ band has two pieces. The upper one is very sharp and peaks at -15.7 eV, resembling that in MgO; the lower piece is about 1.5 eV wide and has two peaks at -17.5 and -16.9 eV. Analysis of the wave function at Γ indicates that the lowest band involves hybridization of O $2s$ and Al $3s$ orbitals; the next lowest band involves the O $2s$ and Mg $3s$ interaction; while the much more localized O $2s$ bands constitute the sharp peak in the DOS at -15.7 eV.

The calculated information on the band structures for the three crystals is listed in Table II.

It is tempting to see if the electronic structure of a complex oxide such as the spinel $MgAl_2O_4$ can be mimicked by that of MgO and α-Al_2O_3. To this end, we plot the broadened DOS of $MgAl_2O_4$ and compare it with the sum of the DOS of MgO and α-Al_2O_3 in Fig. 8. Although the general shapes of the two curves are similar, there is a lack of close agreement. $MgAl_2O_4$ has a much narrower VB width. This is most likely due to the difference in the NN distances. The Mg—O bond length (1.919 Å) in $MgAl_2O_4$ is shorter than that in MgO (2.102 Å), implying a stronger bond thus a narrower band. α-Al_2O_3 has two Al—O lengths of 1.969 and 1.857 Å versus only one type (1.929 Å) in $MgAl_2O_4$, which accounts for a broader VB width in α-Al_2O_3. The structures in the CB are also different. Most prominently, the deep minimum

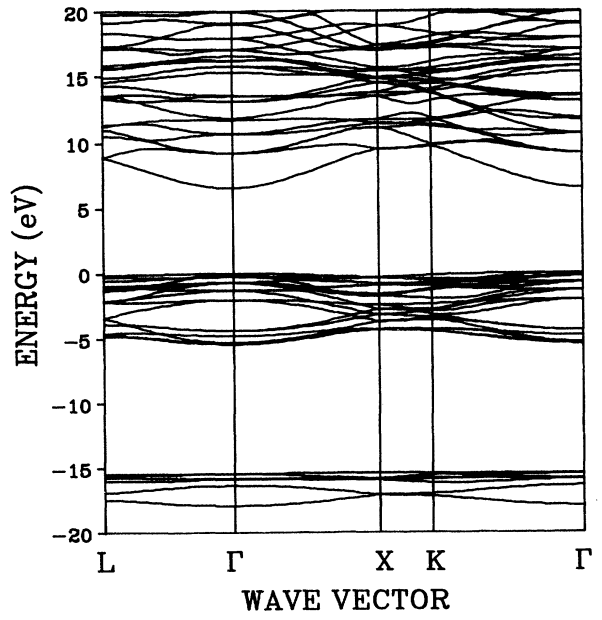

FIG. 6. Band structure of $MgAl_2O_4$.

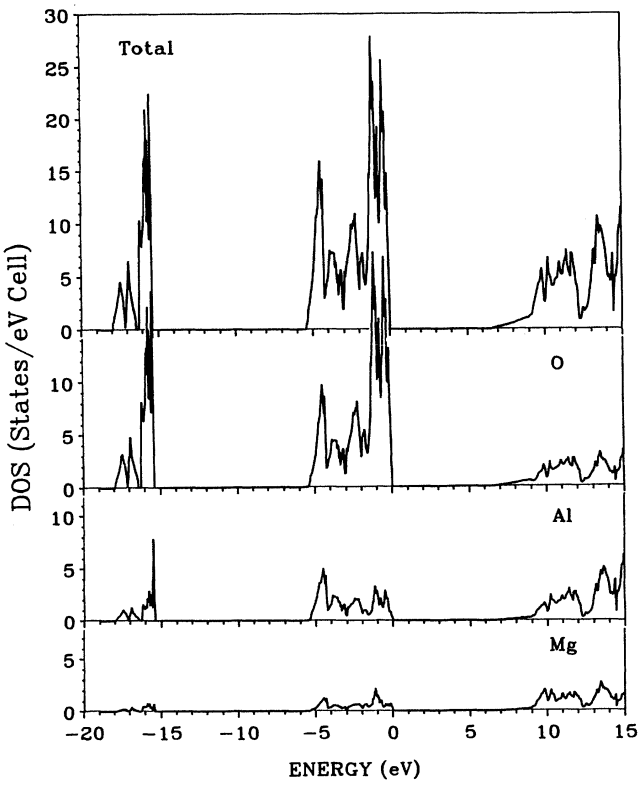

FIG. 7. DOS and PDOS of $MgAl_2O_4$.

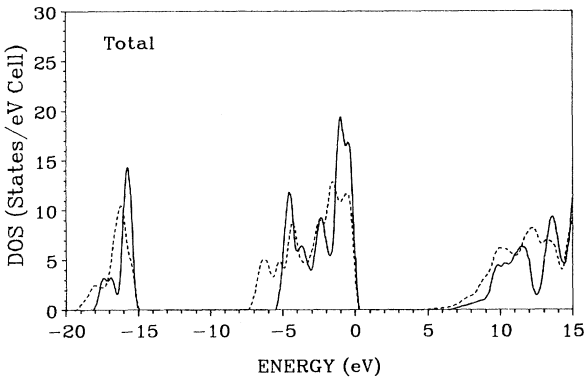

FIG. 8. Comparison of broadened total DOS: solid line, as calculated for $MgAl_2O_4$; dashed line, superposition of MgO and α-Al_2O_3.

at 12.3 eV in $MgAl_2O_4$ is totally absent in the combined DOS of MgO and α-Al_2O_3. Even for the much more localized O $2s$ band, $MgAl_2O_4$ has a sharper leading edge and a narrower bandwidth than the superimposed curve. We therefore conclude that for a precise determination of the electronic structure of a complex oxide, it is necessary to perform a first-principles calculation for the phase considered, instead of deducing it from the electronic structures of the other simpler structures.

V. CHARGE DISTRIBUTION

The charge-density distribution in oxide compounds is an important subject because it relates directly to the effective ionic charges on the ions which play a major role in ionic conductivity. The oxidation state of the ions in a compound is also related to the effective ionic charge. However, the concept of effective ionic charge is not a precisely defined one because of the difficulty in partitioning the charge distribution in real space of the crystalline unit cell. In an empirical type of study and in point-defect models, it is generally taken for granted that the ions take full integral values of charge such as Mg^{2+}, Al^{3+}, O^{2-}, etc., which are probably more appropriate for the description of oxidation states. There has been much dispute on the effective charges on Mg and O in MgO from various calculations ranging from the pure ionic picture of $Mg^{2+}O^{2-}$ (Refs. 5 and 6) to a more covalent picture of Mg^{1+} O^{1-}.[10]

In the LCAO type of calculation, it has been very popular to use the Mulliken population-analysis scheme[37] to estimate the effective charges on each atom. However, the Mulliken scheme is only approximate since it assumes an equal sharing of the overlap integrals between two different atoms. The scheme works quite well for systems in which the atomic wave functions used in the expansion are not too extended such as in minimal-basis-type calculations.[38] However, in-a more accurate calculation, a full basis and beyond is more likely to be used. In this case, the Mulliken analysis can lead to erroneous results because its deficiency becomes more acute due to the extended nature of the basis functions. The effective Mulliken charges calculated for MgO, α-Al_2O_3, and $MgAl_2O_4$ in the present case using a full basis set are listed in Table III. These numbers show very little charge transfer from the cations to anions and are obviously not correct in reflecting the ionic nature of these crystals. In MgO, it wrongly predicts a slight charge transfer from the O to the Mg ion. Batra's calculation[16] on α-Al_2O_3 using the Mulliken scheme also showed very small charge transfer from Al to O. Since the projection of PDOS into partial components uses the Mulliken scheme, the PDOS presented in Sec. VII are qualitative at most.

In this paper, we show that a much more reliable way to obtain the effective charges on each ion is to perform a real-space integration on the charge densities obtained from the self-consistent band calculations. In the OLCAO method, the potential function has no artificial spherical boundary which has been the source of arbitrariness in determining the effective charges in some other methods. Also, the final self-consistent charge density is in a convenient form of a sum of atom-centered Gaussian functions. Still, this process is also approximate because there is no precise way of partitioning the charge in the real space. We assume an average spherical distribution of charge for each ion and integrate the $\rho(\mathbf{r})$ up to an effective ionic radius determined by inspecting the two-dimensional contour charge plots. We impose the constraint that the integrated charges in spheres plus a small amount of interstitial charge must add up to the total charge in the unit cell. The charge density for MgO along a Mg—O bond and on the (001) plane are shown in Figs. 9(a) and 9(b). We determine the effective ionic radius for the Mg and O ions to be 0.358 and 1.243 Å, respectively, which give the integrated effective charges on Mg and O ions to be 0.06 and 7.71 electrons, respectively. This indicates that MgO is highly ionic with almost all of the valence electrons on Mg transferred to O. This assignment leaves 0.23 electrons per unit cell in the interstitial region of the crystal. Dividing this interstitial charge equally among Mg and O ions, we may write the ionic description for MgO as $Mg^{1.83+}O^{1.83-}$.

For α-Al_2O_3 in the rhombohedral lattice, there is no simple crystalline plane that contains both the Al and O

TABLE III. Charge-density distribution in MgO, α-Al_2O_3, and $MgAl_2O_4$.

	MgO	α-Al_2O_3	$MgAl_2O_4$
Mulliken charge (elec.)			
Mg	2.64		1.96
Al		2.70	3.01
O	5.36	6.20	6.01
Integrated charge (elec.)			
Mg	0.06		0.09
Al		0.19	0.25
O	7.71	7.57	7.64
Interstitial charge (elec.)	0.23	1.82	1.70
Total charge in cell (elec.)	8	48	64
Ionic radius (Å)			
Mg	0.358		0.345
Al		0.678	0.695
O	1.243	1.170	1.220

ions. We plot the charge density along the short Al—O bond and on a plane which contains two O and one Al ion as shown in Fig. 10. From the line charge of Fig. 10(a), it appears that the minimum in $\rho(\mathbf{r})$ is at 0.4 Å from the Al nucleus and we may take this value as the effective ionic radius of Al. By inspecting the contour plot of Fig. 10(b), we see that the effective ionic radius of Al has to be larger than 0.4 Å because of the discernible near-spherical distribution of charge around the Al ions beyond the 0.4-Å radius. According to this diagram, we estimate the effective ionic radii for Al and O ions in α-Al_2O_3 to be 0.678 and 1.170 Å, respectively. The integrated effective charges are then 0.19 electrons for Al and 7.57 electrons for O. This assignment accounts for 96.2% of the 48 valence electrons in the unit cell, leaving 1.82 electrons in the interstitial region of the cell. This charge calculation indicates that the Al ion is not completely ionized and α-Al_2O_3 is less ionic than MgO. Similar equal partitioning of the interstitial charges between all the atoms in the cell lead to the formula of $Al_2^{2.63+}O_3^{1.75-}$. This calculation also illustrates the importance of having the contour plot to determine the effective radii for the ions. A similar situation has been encountered in the Y_2O_3 compound in which accurate charge integration gives the ionic formula to be $Y_2^{2.16+}O_3^{1.44-}$ rather than a full ionized picture of $Y_2^{3+}O_3^{2-}$.[39]

$MgAl_2O_4$ has a much more complicated crystal structure and charge distribution. Although the Mg-O NN distance in $MgAl_2O_4$ is slightly smaller than that in MgO, the line charges along the Mg—O and Al—O bonds are quite similar to those in MgO and α-Al_2O_3. In Fig. 11, we plot $\rho(\mathbf{r})$ on a plane parallel to the x-y plane at $z = \frac{7}{8}$. This plane does not contain any Mg ions and shows that there is a large low-charge-density channel along the diagonal of the plane between two rows of O ions. The bonding between Al and O resembles that in α-Al_2O_3.

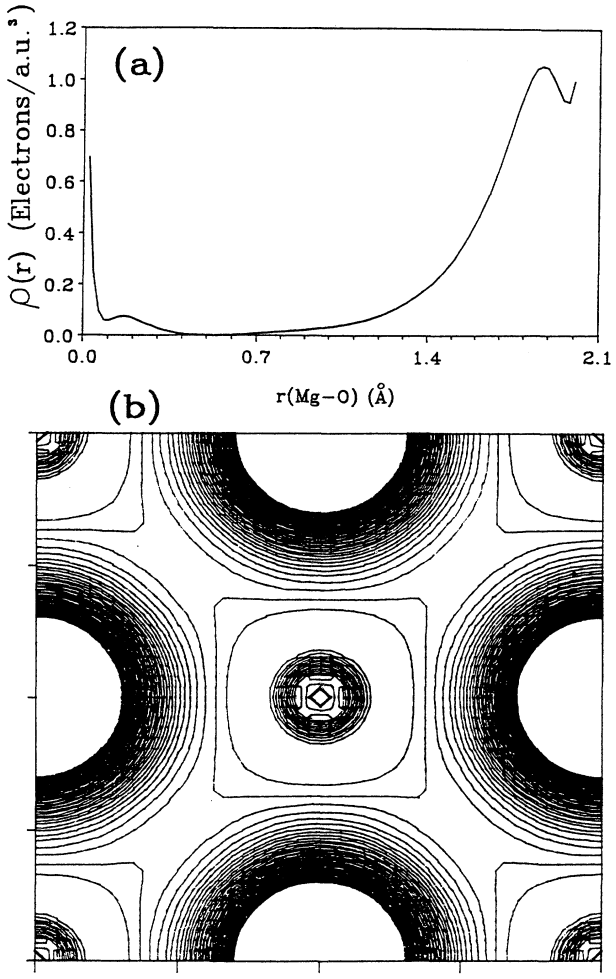

FIG. 9. Charge-density distribution in MgO: (a) along a Mg—O bond of 2.102 Å; (b) in the (001) plane. The contour lines are from 0.01 to 0.25 in the interval of 0.005 in units of electron/(a.u.)^3.

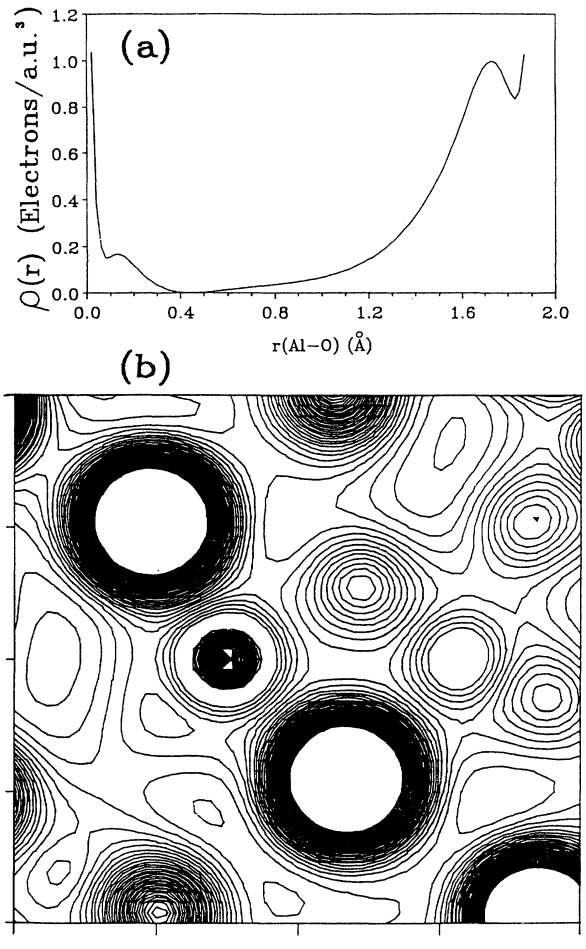

FIG. 10. Charge-density distribution in α-Al_2O_3: (a) along an Al—O bond of 1.969 Å; (b) in a plane containing two O and one Al ion. The contour lines are from 0.01 to 0.25 in the interval of 0.005 in units of electron/(a.u.)^3.

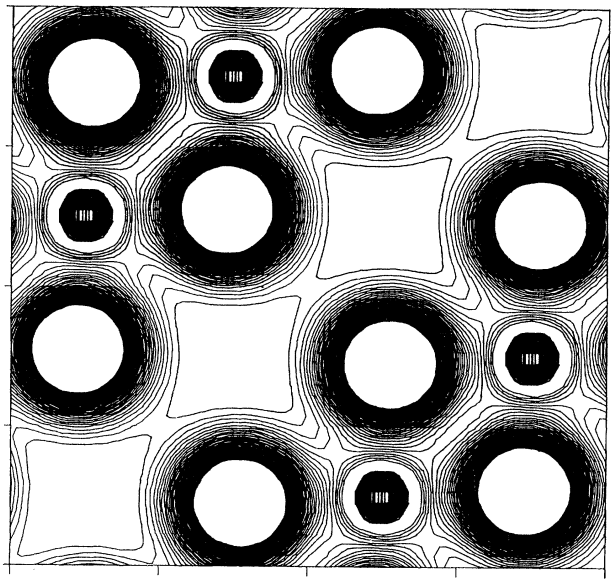

FIG. 11. Charge-density distribution in $MgAl_2O_4$ in a plane parallel to the x-y plane with $z=\frac{7}{8}$ containing only Al and O atoms. The contour lines are from 0.01 to 0.25 in the interval of 0.005 in units of electron/(a.u.)^3.

The next plane with $z=0$ contains only Mg ions at the center and the corners of the plane. The charge density on this plane is shown in Fig. 12. The more or less symmetric pattern of the charge distribution away from the Mg ions comes from the Al and O atoms on the adjacent planes. In Fig. 13 we plot the charge contour on the

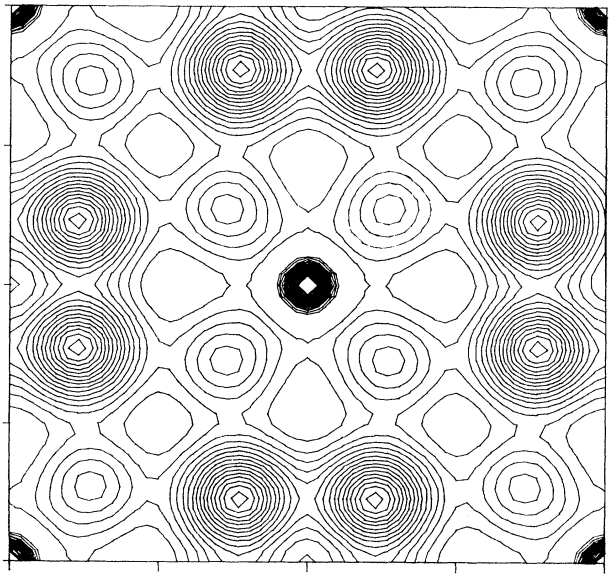

FIG. 12. Charge-density distribution in $MgAl_2O_4$ in a plane parallel to the x-y plane with $z=\frac{0}{8}$ containing only the Mg atoms which are at the center and the corners of the plane. The contour lines are from 0.01 to 0.25 in the interval of 0.005 in units of electron/(a.u.)^3.

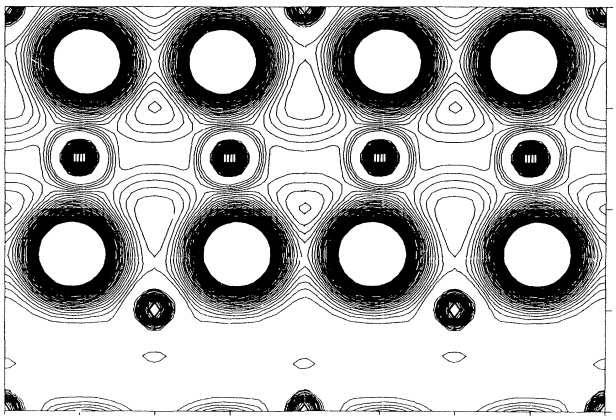

FIG. 13. Charge-density distribution in $MgAl_2O_4$ in the [110] plane. The dark circles at the lower part of the plane near the open channel represent the Mg ions. A layer of Al ions is between two layers of O ions represented by large circles. The contour lines are from 0.01 to 0.25 in the interval of 0.005 in units of electron/(a.u.)^3.

(110) plane which contains all three types of ions. In the lower half of this plane, there is a huge empty channel with almost no or little charge. We expect the small Mg ion to be easily diffused along such a channel. No similar empty channels exist in MgO or α-Al_2O_3 crystals. From Figs. 11 and 12, we estimate the effective ionic radii for Mg, Al, and O ions in $MgAl_2O_4$ to be 0.345, 0.695, and 1.220 Å, respectively. The corresponding integrated charges for each ion are 0.09, 0.25, and 7.64 electrons, respectively. This leaves 1.70 electrons out of a total of 64 electrons in the interstitial region. Again, by equal partitioning of the interstitial charges among the 14 atoms in the primitive cell, we write the ionic formula for the spinel to be $Mg^{1.79+}Al_2{}^{2.63+}O_4{}^{1.76-}$.

VI. OPTICAL ABSORPTION

The optical-absorption measurements on MgO and α-Al_2O_3 have been carried out by several groups in the past.[40–44] Only very recently, using a laser plasma light source and the VUV technique, the reflectivity data in wide-gap insulators can be measured up to 40 eV and higher,[1,2] which ensures a maximum accuracy in converting optical data using the Kramers-Kronig relation. Furthermore, this new experimental setup provides a much higher energy resolution such that smaller structures in the spectrum can be resolved. The availability of high-quality optical data on MgO, α-Al_2O_3, and $MgAl_2O_4$ is part of the motivation for the present theoretical calculation. With experimental data measured up to a high-photon frequency, the interband transitions from very low-lying O 2s bands to the very high CB states can be studied. Previous experimental measurements usually limited the photon energy of less than 10 eV (Ref. 43) because the windowed VUV sources stop at 11 eV.

The first-principles optical calculation within the OLCAO method has been described in considerable de-

tail in our published work on other materials.[27,28,32,39] Generally, the momentum matrix elements between each pair of the occupied VB and the empty CB are calculated at each **k** point in the irreducible portion of the BZ using the Bloch functions from the band calculation. The interband optical conductivity in the dipole approximation is then evaluated by considering all possible pairs of transitions. The summation over the BZ is facilitated by using the linear analytic tetrahedron method.[31] The interband optical conductivity is related to the imaginary part of the dielectric function $\epsilon_2(\omega)$ through $\epsilon_2(\omega) = (4\pi/\omega)\sigma_1(\omega)$. The real part, $\epsilon_1(\omega)$, can be obtained numerically by Kramers-Kronig transformation. The zero-frequency limit of $\epsilon_1(\omega)$ gives the electronic part of the static dielectric constant ϵ_0, a parameter of fundamental importance in many aspects of materials properties.

The calculated imaginary part of the dielectric functions $\epsilon_2(\omega)$ for the three crystals MgO, Al_2O_3, and $MgAl_2O_4$ are shown in Figs. 14, 15, and 16, respectively. Also shown are the experimental VUV data from Ref. 2.

It must be pointed out that in comparing the experimental and the theoretical curves, no shift in the energy scale has been applied. It has been long recognized that the LDA scheme underestimates the band gap in semiconductors and insulators, sometimes up to 50%. A common practice has been to apply an operator to widen the gap so as to match the experimentally reported band gap and shift all the CB states accordingly. This approach has some drawbacks. First, it assumes that the measured gap, usually from some kind of optical experiments, is to be identified with the calculated intrinsic gap. In many instances, this is not the case either because the threshold absorption is symmetry forbidden or is of such a low intensity that it cannot be detected experimentally.[27] Second, it also assumes that all the CB states will be underestimated in energy relative to the VB top by the same amount. The best way to check the validity of this assumption is to compare the calculated and the measured optical transition spectrum with the experimental data up to a very-high-photon energy. Third, in many wide-gap insulators, existence of excitons near the absorption edge greatly complicates the absorption spectrum itself. Since the formation of an exciton is part of the many-body interaction in crystals which is not properly accounted for by the one-electron calculation, the discrepancy in the gap value cannot be totally attributed to the shortcomings of LDA. In the present study, we are surprised to find that for the three crystals we studied, there is no need to apply such a shift to align the major structures beyond the threshold in the absorption curves. Apparently, the formation of an exciton has

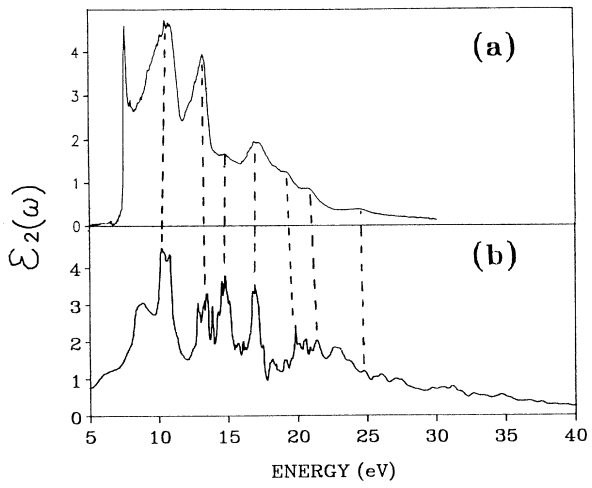

FIG. 14. Imaginary part of the dielectric function $\epsilon_2(\omega)$ for MgO: (a) experimental data from Ref. 2; (b) present calculation.

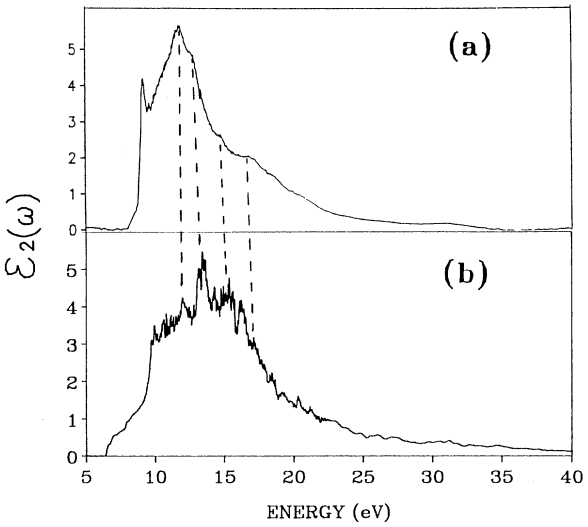

FIG. 15. Imaginary part of the dielectric function $\epsilon_2(\omega)$ for α-Al_2O_3: (a) experimental data from Ref. 2; (b) present calculation.

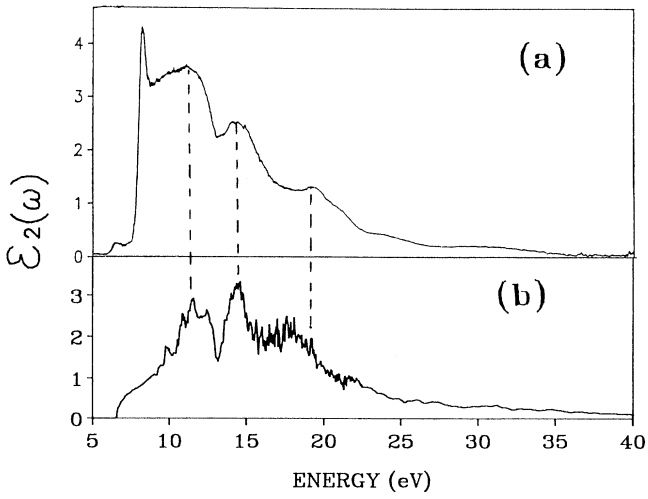

FIG. 16. Imaginary part of the dielectric function $\epsilon_2(\omega)$ for $MgAl_2O_4$: (a) experimental data from Ref. 2; (b) present calculation.

somehow modified the absorption-edge profile, making it much sharper than predicated by the one-electron calculation. However, the major absorption features beyond the excitonic peak are quite well accounted for by the one-electron LDA calculation.

For MgO, the experimental $\epsilon_2(\omega)$ curve in Fig. 14(a) shows an excitonic peak at 7.7 eV with a very sharp absorption edge. The main spectrum shows three major peaks at 10.6, 13.3, and 17.1 eV with smaller structures at 14.9, 19.2, 20.8, and 27.0 eV. These structures are generally well reproduced by the calculation except relative intensities of the structures are somewhat off. There are no other prominent absorption structures beyond 25 eV. The overall magnitude of the $\epsilon_2(\omega)$ curve is also in good agreement with experiment. The new data of Ref. 2 on MgO are actually quite similar to the much earlier measurement of Roessler and Walker.[40] The main difference is that the leading peak at 10.6 eV is now higher than the second peak near 13 eV. We also note that our assignment of the peak structures is different from that of Fong, Saslow, and Cohen,[45] who used the empirical pseudopotential band structures to calculate the $\epsilon_2(\omega)$ curve.

For α-Al_2O_3, the excitonic peak is at 9.2 eV and the experimental curve shows a single major peak at 11.8 eV. Some weak shoulder structures at 12.6, 14.8, and 16.9 eV are also discernible. Beyond 20 eV, there is very little absorption. The calculated curve reproduces these features very well except for the fact that the calculated profile appears to be a bit too broad. But again, the overall magnitude is in very good agreement with the experimental curve. The experimental optical gap for α-Al_2O_3 was quoted as 8.8 eV as determined from the cutoff of the transmission data.[1] However, the absorption coefficient curve actually shows the threshold to be at 6.4 eV, very close to the calculated gap. French has attributed this as arising from the charge-transfer transitions from Cr impurities.[1] Arakawa and Williams[43] had also measured the optical properties of single-crystal α-Al_2O_3 in the vacuum-ultraviolet region. Although the general features of the spectrum are quite similar, their data are much less resolved than that of Ref. 2.

For $MgAl_2O_4$, a sharp excitonic peak exists at 8.2 eV. Unlike MgO, there appears to be a small absorption structure at 6.4 eV below the excitonic peak. It is not clear whether this is due to the interband absorption or some other mechanisms such as phonon-assisted transitions to impurity or defects states in the gap. The experimental $\epsilon_2(\omega)$ curve for $MgAl_2O_4$ shows three very broad peaks at 11.1, 14.2, and 19.2 eV. Beyond 25, eV, the absorption is negligible. These features are again well reproduced by the calculation except the relative intensities of the peaks are in lesser agreement. It is also clear that the $\epsilon_2(\omega)$ curve for $MgAl_2O_4$ has no resemblance to the average $\epsilon_2(\omega)$ curves of MgO and α-Al_2O_3.

Apart from the complications due to the existence of the excitonic peaks near the absorption edges, the overall agreement between theory and experiment for the optical absorptions up to 40 eV for all three crystals is quite good. The calculation does show more structures in the spectra. However, it should be remembered that the calculation is essentially for a crystal at zero temperature, while the real measurement may be affected by the presence of phonons at finite temperature such that some of the finer structures may not be well resolved.

In Fig. 17 we display the real part of the dielectric function for the same three crystals as obtained from $\epsilon_2(\omega)$ by the Kramers-Kronig transformation. All three curves have very similar features. The most important information is the value of $\epsilon_1(\omega)$ in the limit of zero frequency. This corresponds to the electronic part of the static dielectric constant of the material. Our calculated values of ϵ_0 for MgO, α-Al_2O_3, and $MgAl_2O_4$ are 4.28, 3.86, and 6.07, respectively, which are also listed in Table II. Our calculation shows that α-Al_2O_3 has the lowest dielectric constant and $MgAl_2O_4$ the highest among the three crystals. Thus ϵ_0 for $MgAl_2O_4$ does not interpolate between the corresponding values from MgO and α-Al_2O_3. However, the calculated value of ϵ_0 will also be sensitive to the gap value. If the band gap is increased, ϵ_0 will decrease and vice versa. In a capacitance type of measurement to determine the dielectric constant of a material, ϵ_0 values will be significantly affected by electron-phonon interactions, and the measured ϵ_0 values

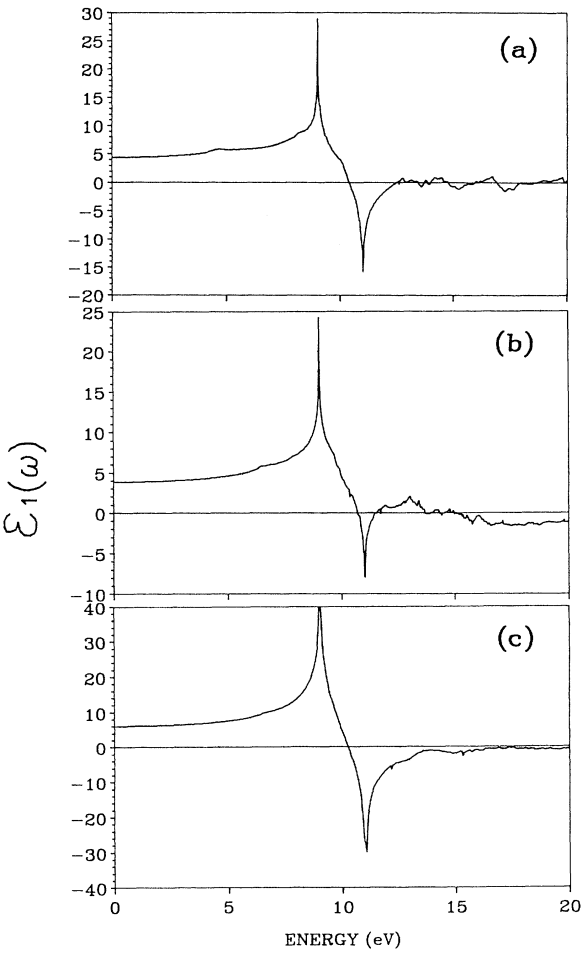

FIG. 17. Real part of the dielectric function $\epsilon_1(\omega)$ for (a) MgO, (b) α-Al_2O_3, and (c) $MgAl_2O_4$.

will be larger than the calculated ones which accounts only for the electronic part alone.

VII. DISCUSSION

We have presented the results of first-principles studies of the electronic and optical properties of three important oxide crystals, namely, MgO, α-Al_2O_3, and $MgAl_2O_4$. This is the first time the electronic structure of the spinel has been studied, together with MgO and α-Al_2O_3 using the same computational method. A number of important electronic parameters such as the bandwidth, band gaps, effective masses, etc., using the LDA are obtained. For all three crystals, the electron effective mass is of the order of less than $0.5m_e$, comparable to most semiconductors and is much smaller than the hole effective mass. This indicates that electronic conduction in these crystals is possible, if somehow the electrons can be promoted to the CB by overcoming the large band gap.

We have also made a detailed analysis of the charge distributions in the three crystals. It is shown that the Mulliken analysis is not adequate for ionic crystals and a direct-space integration scheme gives much more accurate results. MgO is found to be almost fully ionized; α-Al_2O_3 has a slight covalent character and $MgAl_2O_4$ is somewhat intermediate. Ionic formulas of $Mg^{1.83+}O^{1.83-}$, $Al_2^{2.63-}O_3^{1.75-}$, and $Mg^{1.79+}Al_2^{2.63+}O_4^{1.76-}$ are deduced. Detailed contour maps on $MgAl_2O_4$ reveal some open channels of very low electron density in the cubic cell of the spinel structure and it is argued that such open channels may be very important in ionic transport in $MgAl_2O_4$.

The interband optical calculation produced results in surprisingly good agreement with recent data. The presence of excitonic levels in all three crystals has greatly modified the absorption profile near the threshold. This could partly be due to transitions from the VB to the resonant states of the exciton in the CB continuum.[46] The experimental data in the threshold region are further complicated by the possible transitions to the charge-transfer bands due to the trace of impurities[47] which always exist in these oxides. However, for absorption in the energy range beyond the excitonic peak, the agreements between theory and experiments are very good without the need of applying a finite shift in the energy scale. This seems to suggest that the high CB states from the OLCAO-LDA calculation are reasonably accurate. It is a generally accepted notion that the LDA approximation is incapable of giving accurate CB states because it is strictly valid only for the ground state.[48] And this has been the main reason why the band gaps for semiconductors and insulators are always underestimated by the LDA calculation. Another equally valid argument is that the underestimation of the band gap in wide-gap insulators is due to the incomplete cancellation in the self-energy terms in the Coulomb and exchange potentials in the LDA.[48,49] Application of the self-interaction correction to the band-structure calculation of LiF increases the gap value considerably.[50] Our surprisingly good results on MgO, α-Al_2O_3, and $MgAl_2O_4$ may lead to further investigation as to whether this prevailed notion is universally correct, or there are exceptions to this such that the one-electron LDA calculation of the CB in some systems may actually turn out to be more valid than generally believed. It can also mean that the band-gap estimation in some ionic compounds in which the excitons are found near the band edge may be fundamentally different from that in the covalently bonded semiconductors.

We have completed a similar first-principles study of the electronic and optical properties of another very important and related oxide system, silicon dioxide. The band structures of all polymorphic forms of SiO_2 were studied before by Li and Ching[51] using the OLCAO method. That calculation, however, was not self-consistent. The self-consistent OLCAO band structure for α quartz was presented some time ago, showing much improvement.[26] The self-consistent band structures and optical absorptions in all polymorphic forms of SiO_2 have been calculated. The correlation of electronic structure and optical properties to the different short-range orders in various polymorphic SiO_2 turns out to be highly interesting and that work will be published separately.[52]

A final comment we wish to make is that ceramic oxides are usually contaminated with defects and impurities and the properties measured are most likely at room temperature or even higher. Our calculation, on the other hand, is for a perfect crystal at zero temperature. Temperature-dependent optical measurements[2] show the structures in $\epsilon_2(\omega)$ become more broadened and shift in energy as temperature is increased. Our results show that a state-of-the-art quantum-mechanical calculation on a highly idealized situation can already give results in good agreement with measurements on real samples. Further progress is therefore possible by extending the present work to more realistic systems which contain crystal imperfections as well as the effects of finite temperatures. Such studies will greatly aid the fundamental understanding of ceramic materials and enlarge their scope of applications.

ACKNOWLEDGMENTS

This work is supported by the U. S. Department of Energy under Grant No. DE-FG02-84ER45170.

[1]R. H. French, J. Am. Ceram. Soc. **73**, 477 (1990).
[2]M. L. Bortz, R. H. French, D. J. Jones, R. V. Kasowski, and F. S. Ohuchi, Phys. Scr. **41**, 4404 (1990); M. L. Boltz and R. H. French, Appl. Phys. Lett. **55**, 1955 (1989).
[3]M. L. Cohen, P. J. Lin, D. M. Roessler, and W. C. Walker, Phys. Rev. **155**, 992 (1966).
[4]S. T. Pantelides, D. J. Mickish, and A. B. Kunz, Phys. Rev. B **12**, 5203 (1975).
[5]P. F. Walch and D. E. Ellis, Phys. Rev. B **12**, 5920 (1975).
[6]N. Daude, C. Jouanin, and C. Gout, Phys. Rev. B **15**, 2399 (1977).
[7]J. Yamashita and S. Asano, J. Phys. Soc. Jpn. **52**, 3506 (1983).

[8]M. S. T. Bukowinski, J. Geophys. Res. **87**, 303 (1982).
[9]K. J. Cheng and M. L. Cohen, Phys. Rev. B **30**, 4774 (1984).
[10]O. E. Taurain, M. Springborg, and N. E. Christensen, Solid State Commun. **55**, 351 (1985).
[11]B. M. Klein, W. E. Pickett, L. L. Boyer, and R. Zeller, Phys. Rev. B **35**, 5802 (1987).
[12]V. A. Lobatch, B. E. Kulyabin, V. P. Zhukov, and N. I. Medvedeva, Phys. Status Solidi B **158**, 239 (1990).
[13]M. Causa, R. Dovesi, C. Pisani, and C. Roetti, Phys. Rev. B **33**, 1308 (1986); **34**, 2939 (1986).
[14]M. H. Reily, J. Phys. Chem. Solids **31**, 1041 (1970).
[15]R. A. Evarentov, A. N. Ermoshkin, and V. A. Lovchikov, Phys. Status Solidi B **99**, 387 (1980).
[16]I. P. Batra, J. Phys. C **18**, 5399 (1982).
[17]S. Ciraci and I. P. Batra, Phys. Rev. B **28**, 982 (1983).
[18]M. Causa, R. Dovesi, C. Roetti, E. Kotomin, and V. R. Saunders, Chem. Phys. Lett. **140**, 120 (1987).
[19]J. Tossell, J. Phys. Chem. Solids **31**, 1273 (1975).
[20]S. Nagel, J. Phys. C **18**, 3673 (1985).
[21]X. Shangda, Guo Changxin, Lin Libin, and D. E. Ellis, Phys. Rev. B **35**, 7671 (1987).
[22]F. S. Galasso, *Structure and Properties of Inorganic Solids* (Pergamon, New York, 1970).
[23]B. N. Harmon, W. Weber, and D. R. Hamann, Phys. Rev. B **25**, 1109 (1982).
[24]W. Y. Ching and B. N. Harmon, Phys. Rev. B **34**, 5305 (1986).
[25]F. Zandiehnadem, R. A. Murray, and W. Y. Ching, Physica B **150**, 19 (1988).
[26]W. Y. Ching and Y.-N Xu, in *SiO_2 and its Interfaces,* edited by S. T. Pantelides and G. Lucovsky, Materials Research Society, Symposium Proceedings Vol. 105 (MRS, Pittsburgh, 1988), p. 181.
[27]W. Y. Ching, Y.-N. Xi, and K. W. Wong, Phys. Rev. B **40**, 8111 (1989).
[28]Y.-N. Xu and W. Y. Ching, Phys. Rev. B **41**, 5471 (1990).
[29]F. Zandienhnadem and W. Y. Ching, Phys. Rev. B **41**, 12 162 (1990).
[30]W. Kohn and L. J. Sham, Phys. Rev. **140**, A1133 (1965).
[31]G. Lehmann and M. Taut, Phys. Status Solidi **54**, 469 (1972); O, Jesen and O. K. Andersen, Solid State Commun. **9**, 1763 (1971); J. Rath and A. J. Freeman, Phys. Rev. B **11**, 2109 (1975).
[32]G.-L. Zhao, W. Y. Ching, and K. W. Wong, J. Opt. Soc. Am. B **6**, 505 (1989).
[33]L. Fiermans, R. Hoogewijs, G. de Meyer, and J. Vennik, Phys. Status Solidi A **59**, 569 (1980).
[34]S. P. Kowalcyzk, F. R. McFeely, L. Ley, V. T. Gritsyna, and D. A. Shirley, Solid State Commun. **23**, 161 (1977).
[35]A. Balzarotti and A. Bianconi, Phys. Status Solidi **6**, 689 (1976).
[36]G. Drager and J. A. Leiro, Phys. Rev. B **41**, 12 919 (1990).
[37]R. S. Mulliken, J. Am. Chem. Soc. **23**, 1833 (1955).
[38]M.-Z. Huang and W. Y. Ching, J. Phys. Chem. Solids **46**, 977 (1985).
[39]W. Y. Ching and Y.-N. Xu, Phys. Rev. Lett. **65**, 895 (1990).
[40]D. M. Roessler and W. C. Walker, Phys. Rev. **159**, 733 (1967).
[41]E. Loh, Solid State Commun. **2**, 269 (1964).
[42]G. H. C. Freeman, Brit. J. Appl. Phys. **16**, 927 (1965).
[43]E. T. Arakawa, and M. W. Williams, J. Phys. Chem. Solids **29**, 735 (1968).
[44]E. R. II'mas and A. I. Kuznetsov Fiz. Tverd. Tela (Leningrad) **14**, 1464 (1972) [Sov. Phys.—Solid State **14**, 1255 (1972)].
[45]C. Y. Fong, W. Saslow, and M. L. Cohen, Phys. Rev. **168**, 992 (1968).
[46]U. Rossler, in *Rare Gas Solids,* edited by M. L. Klein and J. A. Venables (Academic, New York, 1976), p. 505.
[47]H. H. Tippins, Phys. Rev. B **1**, 126 (1970).
[48]J. P. Perdew and M. Levy, Phys. Rev. Lett. **51**, 1884 (1983); L. J. Sham and M. Schluter, *ibid.* **51**, 1888 (1983).
[49]A. Zunger, J. P. Perdeew, and G. L. Oliver, Solid State Commun. **34**, 933 (1980); J. P. Perdew and A. Zunger, Phys. Rev. B **23**, 5048 (1981).
[50]R. A. Heaton and Chun C. Lin, J. Phys. C **17**, 1853 (1984).
[51]Y. P. Li and W. Y. Ching, Phys. Rev. B **31**, 2172 (1985).
[52]W. Y. Ching and Y.-N Xu (unpublished).